Published in final edited form as:
Neurosurgery. 2014 June ; 74(6): 682–696. doi:10.1227/NEU.0000000000000331.

Utilization of Cone-Beam Computed Tomographic Angiography in Planning for Gamma Knife Radiosurgery of Arteriovenous Malformations: A Case Series and Early Report

Mina G. Safain, M.D.[1], **Jason P. Rahal, M.D.**[1], **Ami Raval, M.D.**[1], **Mark J. Rivard, Ph.D**[2,3], **John Mignano, M.D., Ph.D**[2,3], **Julian Wu, M.D**[1,3], and **Adel M. Malek, M.D., Ph.D.**[1,3]

[1]Cerebrovascular and Endovascular Division, Department of Neurosurgery, Tufts Medical Center and Tufts University School of Medicine, Boston, MA

[2]Department of Radiation Oncology, Tufts Medical Center and Tufts University School of Medicine, Boston, MA

[3]Boston Gamma Knife Center, Boston, MA

Abstract

Background—The effectiveness of Gamma Knife radiosurgery (GKR) for cerebral arteriovenous malformations (AVM) is predicated on inclusion of the entire nidus while excluding normal tissue. As such, GKR may be limited by the resolution and accuracy of the imaging modality used in targeting.

Objective—We present the first case series to demonstrate the feasibility of utilizing ultra-high-resolution C-arm cone beam computed tomography angiography (CBCT-A) in AVM targeting.

Methods—From June 2009 to June 2013, CBCT-A was utilized for targeting of all patients with AVMs treated with GKR at our institution. Patients underwent Leksell stereotactic head frame placement followed by catheter-based biplane 2-D digital subtraction angiography (DSA), 3-D rotational angiography (3DRA), as well as CBCT-A. The CBCT-A dataset was used for stereotactic planning for GKR. Patients were followed up at 1, 3, 6, and 12 months, and then annually thereafter.

Results—CBCT-A-based targeting was used in twenty-two consecutive patients. CBCT-A provided detailed spatial resolution and sensitivity of nidal angioarchitecture enabling treatment. The average radiation dose to the margin of the AVM nidus corresponding to the 50% percent isodose line was 15.6 Gy. No patient had treatment-associated hemorrhage. At early follow-up (mean=16 months), 84% of patients had a decreasing or obliterated AVM nidus.

Conclusion—CBCT-A-guided radiosurgery is feasible and useful because it provides sufficient detailed resolution and sensitivity for imaging brain AVMs.

Corresponding author: Adel M. Malek, MD, PhD Department of Neurosurgery Tufts Medical Center 800 Washington Street Proger 7 Boston, MA 02111 Tel: 617-636-8200 Fax: 617-636-7587 amalek@tuftsmedicalcenter.org.

Disclosures: The other authors report no conflict of interest concerning the materials or methods used in this study or the findings specified in this paper. This manuscript has not been previously published in whole or in part or submitted elsewhere for review.

Keywords

arteriovenous malformation; cone beam computed tomography; Gamma Knife Radiosurgery; stereotactic radiosurgery

INTRODUCTION

The main treatment modalities for arteriovenous malformations (AVM) include microsurgical resection, endovascular embolization, and stereotactic radiosurgery (SRS). SRS has become an increasingly useful treatment option for AVM when surgical risks are thought to be excessive. Overall, the reported rate of angiographic AVM obliteration at an average of two years after SRS has been reported to vary from 60% to 85%[1-9]. Gamma knife radiosurgery (GKR), one type of SRS, has been shown to have a high degree of conformity to a lesion as well as minimize low-dose spread to adjacent normal tissue areas when compared to linear accelerator-based therapies[10-13]. This is due to the lower energy of the radiation source allowing a more precise ability to target a lesion and decrease the amount of radiation given to surrounding healthy tissue. However, GKR, like other forms of SRS, is dependent on the accuracy of the images supplied for treatment. In addition, higher obliteration rates and lower rates of treatment failure and complications are achieved when inclusion of the entire AVM nidus is accomplished while the venous drainage as well as the arterial feeders are excluded from the radiation field[2, 4, 8, 9]. This makes it important for treating clinicians to have an accurate and detailed visualization of the three-dimensional (3-D) angioarchitecture of the target lesion.

Historically, catheter-based digital subtraction angiography (DSA) has been the main modality in delineating an AVM nidus. However, angiograms are limited in this purpose, as they are two-dimensional representations of a three-dimensional structure[14]. Although still considered the gold standard, DSA has been shown to be prone to errors in terms of nidus size and shape.[15] Several imaging modalities have developed over the years and have added to the visualization of the three-dimensional nidus of AVMs (Table 1). These modalities include CT angiography (CTA), three-dimensional magnetic resonance angiography (3-D MRA) either by time of flight or contrast enhancement, and different catheter-based additions to traditional DSA including subtracted 3-D rotational angiography (3DRA). DSA images have traditionally been used for planning as a stand-alone image set or with fusion to either stereotactic CT or MRI images. More recently, treatment planning has been shown to be more precisely accomplished using 3DRA as compared to standard CT/MRI fusion-based contouring[16].

C-arm cone beam computed tomography angiography (CBCT-A) technology has been used to detect intraluminal thrombus, plaque morphology, as well as define vascular architecture, but its use in GKR planning for treatment of AVMs has not been evaluated or reported in detail[17-20]. Since June 2009, we have routinely used CBCT-A as the imaging platform for all AVMs treated at our center given its higher soft tissue delineation and the exquisite detail it provides of the nidal angioarchitecture. In the current study we present our consecutive case series of patients with AVMs treated utilizing CBCT-A in planning. In addition, we

review the different radiographic modalities and their relative strengths and weakness in the treatment of AVMs.

METHODS

Case Selection

From June 2009 to June 2013, CBCT-A was used for targeting in the treatment planning process for all patients with AVMs treated with GKR at our institution. Prior to June 2009, CTA, MRI/A, and DSA were used alone or in combination to target AVMs for GKR. These patients are not included in this series. Patients' medical charts, radiographic studies, endovascular procedures, and SRS treatment reports were retrospectively reviewed for pertinent history. Variables recorded included patient age, gender, patient presentation, AVM location, size of nidus, Radiosurgery Based AVM Grading Score (RBAS, (0.1*volume, cc) + (0.02*age, years) +(0.5*location))[21], Spetzler-Martin grade, presence of pretreatment hemorrhage, GKR dose, clinical follow-up (including the need for further treatment), and radiographic follow-up. This study was approved by the Institutional Review Board of Tufts Medical Center.

Procedure

On the GKR treatment day, patients had a Model G Leksell stereotactic head frame (Elekta AB, Stockholm, Sweden) placed under local anesthesia and then underwent diagnostic cerebral angiogram that included biplane 2D-DSA, 3DRA, as well as CBCT-A imaging performed on the Siemens Axiom-Artis VB22N 060907 system. The Leksell frame was attached to the angiographic table as to not allow patient motion and significantly limit motion artifact during image acquisition. 3DRA was performed using 3 mL/s of contrast medium for 5 seconds with a 1.5-second preinjection delay; CBCT-A was performed using a 20-second acquisition while injecting contrast medium at 1 mL/s with a 2.0-second preinjection delay (Isovue-250, Bracco Imaging SpA). In each case, AVM nidus size, arterial feeding branches, venous drainage, and anatomical localization were noted. The CBCT-A volumes were reconstructed using maximum intensity projection multiplanar reconstruction (MIP MPR) on a Leonardo/Syngo workstation (Siemens AG, Munich, Germany) and Osirix medical imaging software (OsiriXMD, Geneva, Switzerland).

After the angiogram was completed, CBCT-A images were loaded into the Leksell stereotactic planning computer workstation with Leksell Gamma Plan software LGP v. 8.3.1(Elekta AB, Stockholm, Sweden). CBCT-A images were used for nidus definition. One treatment plan was developed by two neurosurgeons (J.W. and A.M.M.), a radiation oncologist (J.M.), and a radiation physicist (M.J.R.). The nidus size, arterial, and venous anatomy were studied carefully on all three imaging planes. The nidus was outlined in the treatment planning system. Care was made to minimize radiation dose to the draining veins as well as the parent feeding arteries. All GKR treatments were accomplished on the Leksell Gamma Knife model 4C (ElektaAB). After treatment, patients had the stereotactic head frame removed and were discharged home the same day.

Patient Follow-up

Following GKR treatment of an AVM, patients were scheduled for follow-up at 1 month, 6 months, 12 months, and annually thereafter with either an MRI/A or CTA performed at 6 months and an angiogram performed at 1-2 years. At each visit, patients were screened for headaches, any neurologic changes, seizures, or change in daily function. Radiographic studies were reviewed for AVM nidus size or obliteration, development of perilesional edema, and the remaining arterial and venous anatomy of the AVM. We divided post-treatment AVM size into three categories: obliterated, decreased in size, or stable in size. Obliteration was determined by DSA in all cases; non-invasive modalities were used to determine stability and decreasing AVMs. All images were reviewed by both a neurosurgeon and a neuroradiologist.

RESULTS

Twenty-two (22) consecutive patients underwent CBCT-A and then GKR therapy for their AVM (Table 2). All patients were consistently found to have detailed visualization of their AVM nidus, feeding arteries, and draining veins on CBCT-A imaging (Fig. 1-6). In all cases the soft tissue delineation was qualitatively improved when compared to DSA, 3DRA, and in some patients non-invasive modalities such as CTA and MRI/A. There were thirteen (59%) males and nine (41%) females. The average age was 43.1years (range 19-61 years). Patients presented with multiple clinical findings including hemorrhage (9 patients, 41%), seizure (8 patients, 36%), headache (3 patients, 14%), and two (9%) patients presented incidentally. Three patients (cases 2, 16, and 22) had previous endovascular embolization. Two patients underwent proton beam therapy at an outside institution prior to presentation (cases 4 and 18). No patient in this cohort had previous surgery.

The average maximal nidus diameter was 2.19 cm (range 1.0-4.5 cm) and anatomic location was varied throughout the cerebrum. The average modified RBAS[21] was 1.17 (range 0.44-2.14). Most AVMs had Spetzler-Martin grades of 2 and 3, although one patient had a grade 4 AVM. All but three patients had AVMs that were located within eloquent cortex. The average radiation dose to the margin of the AVM nidus corresponding to the 50% percent isodose line was 15.6Gy (range 12-20 Gy).

Average follow-up (Table 3) for this prospectively maintained cohort was 16 months (range 0-39 months). Two patients (10%) were lost to follow-up. All patients experienced improvement in their clinical symptoms. In this cohort and at current follow-up, we have had no treatment-associated hemorrhage. Four patients (18%) had an increase in their seizure frequency after GKR treatment. In our patient cohort with follow-up greater than 1 month (18 patients), five patients (28%) had no residual AVM visualized, ten patients (56%) had a decreasing size of the nidus, and three patients (17%) had stable size of the AVM nidus. Since this was a prospectively maintained cohort with modest follow-up times, most obliterated AVMs have occurred in the earlier cases, decreasing-sized AVMs are in the middle of the cohort, and stable-sized AVMs are at the end of the cohort.

One patient had moderate radiation associated MRI T2 change that occurred 20 months after treatment. This was treated with 2 weeks of steroids and the edema has been decreasing on

follow-up MRI studies. No patients have developed necrosis. No patients have required additional surgery, embolization, or retreatment with GKR.

DISCUSSION

SRS-associated treatment failure has been associated with many factors. The most prominent failure is targeting error,[2, 4, 8, 9] which is the most common reason for residual AVM. In addition, although uncommon, hemorrhage due to residual nidus or radiation to the venous drainage of an AVM has been reported after SRS. [3, 7, 22-24] It is therefore beneficial during treatment to have the best radiographic 3-D understanding of an AVM's nidus as well as of the feeding arteries and draining veins in order to achieve the highest success of AVM obliteration.

Methods for Visualizing AVMs

Different visualization techniques including CTA, 3-D-MRA, DSA, and 3DRA, have been reported to be used in the operative planning for AVMs[14, 15, 25] (Table 1). These different techniques have been demonstrated to provide different AVM volumes for radiosurgery targeting.[14, 26, 27] 3-D-MRA has proven satisfactory for operative planning given its superiority in providing a full 3-D visualization of an AVM nidus.[14, 28-30] However, 3-D-MRA has been noted to be heavily affected by clip artifact as well as not allowing temporal resolution of an AVM.[14] In addition, 3-D-MRA has a significantly lower spatial resolution than DSA[31, 32]. For these reasons, DSA has remained the gold standard for operative planning for stereotactic radiosurgery. DSA, however, has been criticized because the acquired 2-D images do not provide the full 3-D lesion visualization required for proper preoperative targeting.[14] Therefore, recent studies have described potential solutions to these limitations through co-registration of multiple imaging modalities including 2-D-DSA images and the 3-D spatial relationships provided by MRA and CTA.[26, 27, 33, 34]

Subtracted 3DRA has tried to eliminate the shortcomings of 2-D-DSA and has been found to be useful for AVM targeting by providing greater information about the feeding arteries and AVM filling patterns[35-37]. Selective catheterization and 3DRA can enable identification of separate AVM compartments,[36] giving the clinician a greater 3-D understanding for successful planning. However, 3DRA has the disadvantage of spatial distortion of 3-D images, making it less reliable when used alone. In addition, it is not feasible to image the entire Leksell head frame on certain systems during acquisition of the 3DRA images, and therefore it cannot be used alone in administering therapy. This data, however, can then be co-registered with DSA, CT, or MRI, therefore providing a reference imaging modality from which to administer therapy.[38]

CBCT-A as a new tool in the visualization and treatment of AVMs

The relatively recent addition of CBCT-A technology to the neurointerventional suite will likely have a major impact on AVM visualization and subsequent targeting for GKR. Several studies have demonstrated that the addition of flat panel detectors to the neurointerventional suite enables higher acquisition speeds and CT-quality contrast resolution of the intracranial vasculature.[39-41] CBCT-A has been noted to have detailed

spatial resolution including being able to resolve submillimeter objects such as stent struts measuring 50-70μm[39]. In addition, CBCT-A has been especially efficient in imaging the morphological characteristics of contrast-injected vessels and their relationship to bony structures with greater spatial resolution than would be otherwise available on the procedure table (Fig 1, 2, 4 and 5).[42] Furthermore, CBCT-A can be applied to 3-D datasets and multi-planar reconstructions in the same fashion as spiral CT datasets, transferring the high spatial resolution of CBCT-A to the application of AVM targeting.[43] This allows the clinician to use this one dataset without the need for co-registration with another 3-D imaging technology. In addition to the aforementioned benefits, CBCT-A enhanced by intra-arterial contrast injection facilitates other benefits as well, such as the detection of micro-alterations to the vasculature indicative of early hemorrhage, hypoperfusion, as well as the identification of hydrocephalus in the peri-procedural time period.[44-46]

Although the benefits of CBCT-A are numerous, the technology has some limitations. First, like other CT modalities, CBCT-A is limited by artifacts caused by metal (clips, stents, or coils) as well as embolic material, causing a star-burst effect which can limit its use in previously treated AVMs. In addition, with respect to safety, a single 20-second CBCT-A acquisition involves the delivery of 22 mL of contrast agent and is associated with approximately a 0.2 Gy radiation dose compared to 3DRA, which involves 18 mL of contrast agent and 0.065 Gy, while a standard DSA run utilizes 6-10 mL of contrast agent and is associated with about 0.15 Gy. Although CBCT-A delivers an increased radiation dose compared to 3DRA and DSA, it is important to be cognizant that utilizing multiple magnified-DSA runs in order to acquire appropriate visualization may deliver a higher dose than a single CBCT-A run. Thus, the overall radiation dose delivered to a patient may, in fact, be higher with the traditional use of multiple DSA runs when compared to the use of one DSA run and an additional CBCT-A acquisition.

In our current experience, we have found that CBCT-A allows extensive and detailed visualization of an AVM nidus as well as improved resolution of the feeding arteries and draining veins within these lesions (Fig 1, 2, 4, and 5). In addition, we have subjectively noted that CBCT-A provides a more detailed resolution of AVMs than other catheter-based modalities such as DSA or 3DRA as well as other non-invasive modalities such as CTA and MRA. We currently treat all AVMs undergoing GKR using CBCT-A as the principle dataset and have not had any patient's AVM not visualized on CBCT-A. Furthermore, we have recently reported on AVMs that were not visualized on any other imaging modalities that were able to be resolved with CBCT-A[20] and present two additional patient in this current series (Fig 3 and 6). CBCT-A has enabled us to treat these lesions where previously repeat angiography at a delayed time point would need to be completed in order to visualize the AVM lesion. Additionally, in some instances even repeat angiography has not been 100 percent sensitive in discovering AVMs, leaving patients at risk of re-rupture of their AVM.

Results of AVM treatment when using CBCT-A

Although we present this series as an initial report of the feasibility and increased spatial resolution of CBCT-A compared to other planning technologies, it is important to consider the early results of this series. This series demonstrates obliterated or decreasing AVM nidus

size in 84% (28% obliterated, 56% decreasing in size) of patients at an average of 16 months follow-up with an average dose of 15.6Gy. Although our current obliteration rate is low, this is likely due to our modest average follow-up of 16 months. Douglas et al.[47] have demonstrated in a single center study of 95 patients a 6-year obliteration rate of 71.4% with 90% of obliterations occurring between 24 and 58 months. Likewise, Fokas et al.[48] in a study of 164 patients demonstrated a median time to obliteration of 29 months with 3- and 5-year obliteration rates of 61% and 88%, respectively. We report no post-treatment hemorrhage, 4.5% (1/22) of patients developing perilesional edema, and no radiation necrosis at an average dose of 15.6Gy. Parkhtik et al. [49], in a study of 102 patients, noted perilesional edema in 43.1% of patients and had 6.9% of patients develop radiation necrosis with an average radiation dose of 18.5 Gy. Similarly the University of Pittsburgh group[50] has reported the development of perilesional imaging changes in approximately 30% of patients in numerous studies. The lower complication rate in the current study is likely the result of lower prescription dose; whether CBCT-A visualization altered the nidus selection and enabled a lower dose is not addressed and cannot be answered with the data provided. In addition, the decreased amount of MRI flair changes in this series may also be due to a lower maximal dose than the actual advantage of CBCT-A in targeting accuracy or venous drainage pathway avoidance. Whether the lower complication rate we report is due to our lower radiation dosing, modest follow-up, or different nidal targeting due to CBCT-A will need further follow-up. Finally, given the modest follow-up, it will be important to further follow these patients for determination of the GKR success rate to obliterate AVMs. We hypothesize that our current number of obliterated AVMs will increase given our relatively short follow-up period and the delayed fashion in which GKR works for AVM therapy. While the study sample is small due to the recent introduction of CBCT-A as a neuroimaging tool, we hope to provide an increased patient sample size as patients are enrolled into our prospective database. Obtaining greater follow-up and a larger patient cohort will assist determination of whether this imaging modality provides superior treatment results compared to standard practice.

Limitations of this Study

Although we report that CBCT-A can resolve nidal, arterial, and venous anatomy of an AVM with significant detail, it is unknown whether using this technique will result in a higher rate of nidus obliteration or change the complication rate when compared to current practice. This extra soft tissue delineation and possibly smaller radiated volume may be more prone to targeting error from slight brain tissue shift during treatment. Additionally, in this series we have intentionally tended towards the lower range of prescription dose compared to published literature. We deliberately adopted this conservative approach hoping to reduce the complications of radiation necrosis and increased peri-lesional edema with an understanding of the drawback of longer time to obliteration and possible lower response rate. Furthermore, although standard treatment of AVMs in both the surgical and radiosurgery arenas tend to advise sparing the draining vein, previous series with SRS to AVMs have not had as detailed visualization of draining veins as in our series, and it may be that in previous treatment plans the draining veins may have received an increased radiation dose compared to our treatments. Multiple series[51-54] have reported on patients developing radiation-induced changes surrounding the treated nidus and a concurrent thrombosis of the

draining vein or veins. In these series, the majority of patients had a favorable outcome implying that some radiation to the draining veins may eventually help with AVM obliteration. In addition, it has been reported in an autopsy study[55] that the draining veins often have the least endothelial damage from SRS, and that some radiation to the proximal draining vein may be beneficial in obliteration of the AVM as long as vein obliteration occurs in a slow and non-acute fashion. Furthermore, it is common to find the draining vein or veins embedded within the nidus and therefore receiving some radiation dose (Fig 2). It is unknown whether some radiation to the draining vein is beneficial to nidus obliteration; this must be studied further.

This study encompasses all the limitations of a retrospective case series. In an ideal setting, CBCT-A would be simultaneously compared in prospective fashion to CTA, MRI/A, and 3DRA on a per-patient basis with treatment volumes analyzed and long-term rates of obliteration assessed. Although this would be the most scientifically sound method of assessing this modality, concerns can arise from exposing patients to additional radiation and contrast as well as gadolinium for research purposes. This may not be readily justified to prove that CBCT-A has improved soft tissue delineation and possibly improved obliteration rates, because of the heterogeneity of AVMs in general and the difficulty in obtaining sufficient samples to compare outcomes from different planning modalities. It may nonetheless enable a comparison of possible treatment volume differences between modalities; the absence of such data in the current report represents a limitation. Another limitation is that our assessment of CBCT-A is qualitative given its retrospective nature and the fact that not every patient received contemporaneous CTA, MRI/A, and 3DRA. Furthermore, in this study we compared the soft tissue delineation of CBCT-A to our institution's CTA. Currently, CT scanner technology is advancing and CBCT-A will need to be compared to the latest 320-detector CT scanner. Finally, our AVM planning was done by all clinicians (J.W., J.M., M.J.R. and A.M.M.) in one sitting without different treatment plans being made by each. This limits us in being able to compare inter-reader differences of the AVM treatment plan.

In this report, we provide the first case series of 22 patients utilizing CBCT-A as the image set for planning of GKR AVM treatment. Although length of follow-up of these patients is currently modest, this report serves to present the feasibility, discuss some advantages of this imaging modality, and demonstrate its applicability to AVM treatment. At this time, CBCT-A should be considered a useful adjunct to other imaging modalities and in those cases in which other imaging modalities are unable to resolve the underlying AVM. Prospective studies evaluating the effectiveness of this modality in comparison to other catheter-based methods, such as 3DRA, as well as simultaneous non-invasive methods such as CTA and MRI/A on a per-patient basis will need to be completed prior to assessing this modality's relative utility in AVM treatment.

CONCLUSION

CBCT-A-guided radiosurgery is feasible and useful because it provides sufficient detailed resolution and sensitivity for imaging brain AVMs. Further study with longer follow-up is

warranted to assess the role and clinical benefit, if any, of this new imaging modality in the treatment of AVMs.

Acknowledgments

This work was supported by NIH-R21HL102685. The senior author (A.M. Malek) has received research funding from Siemens Inc. for imaging-related research.

REFERENCES

1. Foote KD, Friedman WA, Ellis TL, Bova FJ, Buatti JM, Meeks SL. Salvage retreatment after failure of radiosurgery in patients with arteriovenous malformations. Journal of neurosurgery. Feb; 2003 98(2):337–341. [PubMed: 12593620]
2. Ellis TL, Friedman WA, Bova FJ, Kubilis PS, Buatti JM. Analysis of treatment failure after radiosurgery for arteriovenous malformations. Journal of neurosurgery. Jul; 1998 89(1):104–110. [PubMed: 9647180]
3. Friedman WA, Blatt DL, Bova FJ, Buatti JM, Mendenhall WM, Kubilis PS. The risk of hemorrhage after radiosurgery for arteriovenous malformations. Journal of neurosurgery. Jun; 1996 84(6):912–919. [PubMed: 8847584]
4. Gallina P, Merienne L, Meder JF, Schlienger M, Lefkopoulos D, Merland JJ. Failure in radiosurgery treatment of cerebral arteriovenous malformations. Neurosurgery. May; 1998 42(5):996–1002. discussion 1002-1004. [PubMed: 9588543]
5. Karlsson B, Lindquist C, Steiner L. Prediction of obliteration after gamma knife surgery for cerebral arteriovenous malformations. Neurosurgery. Mar; 1997 40(3):425–430. discussion 430-421. [PubMed: 9055280]
6. Pollock BE, Flickinger JC, Lunsford LD, Maitz A, Kondziolka D. Factors associated with successful arteriovenous malformation radiosurgery. Neurosurgery. Jun; 1998 42(6):1239–1244. discussion 1244-1237. [PubMed: 9632181]
7. Pollock BE, Flickinger JC, Lunsford LD, Bissonette DJ, Kondziolka D. Hemorrhage risk after stereotactic radiosurgery of cerebral arteriovenous malformations. Neurosurgery. Apr; 1996 38(4): 652–659. discussion 659-661. [PubMed: 8692381]
8. Yamamoto M, Ide M, Jimbo M, Takakura K, Lindquist C, Steiner L. Neuroimaging studies of postobliteration nidus changes in cerebral arteriovenous malformations treated by gamma knife radiosurgery. Surgical neurology. Feb; 1996 45(2):110–119. discussion 119-122. [PubMed: 8607060]
9. Yamamoto M, Jimbo M, Hara M, Saito I, Mori K. Gamma knife radiosurgery for arteriovenous malformations: long-term follow-up results focusing on complications occurring more than 5 years after irradiation. Neurosurgery. May; 1996 38(5):906–914. [PubMed: 8727815]
10. Gevaert T, Levivier M, Lacornerie T, et al. Dosimetric comparison of different treatment modalities for stereotactic radiosurgery of arteriovenous malformations and acoustic neuromas. Radiotherapy and oncology : journal of the European Society for Therapeutic Radiology and Oncology. Feb; 2013 106(2):192–197. [PubMed: 22884842]
11. O'Brien PF, Fung A. Measured spatial accuracy for linac-based radiosurgery. Medical physics. Jul; 1994 21(7):1145–1147. [PubMed: 7968847]
12. Warrington AP, Laing RW, Brada M. Quality assurance in fractionated stereotactic radiotherapy. Radiotherapy and oncology : journal of the European Society for Therapeutic Radiology and Oncology. Mar; 1994 30(3):239–246. [PubMed: 8209008]
13. Stern RL, Perks JR, Pappas CT, Boggan JE, Chen AY. The option of Linac-based radiosurgery in a Gamma Knife radiosurgery center. Clinical neurology and neurosurgery. Dec; 2008 110(10):968–972. [PubMed: 18617321]
14. Bednarz G, Downes B, Werner-Wasik M, Rosenwasser RH. Combining stereotactic angiography and 3D time-of-flight magnetic resonance angiography in treatment planning for arteriovenous malformation radiosurgery. International journal of radiation oncology, biology, physics. Mar 15; 2000 46(5):1149–1154.

15. Spiegelmann R, Friedman WA, Bova FJ. Limitations of angiographic target localization in planning radiosurgical treatment. Neurosurgery. Apr; 1992 30(4):619–623. discussion 623-614. [PubMed: 1584365]
16. Veeravagu A, Hansasuta A, Jiang B, Karim AS, Gibbs IC, Chang SD. Volumetric Analysis of Intracranial Arteriovenous Malformations Contoured for CyberKnife Radiosurgery With 3-Dimensional Rotational Angiography vs Computed Tomography/Magnetic Resonance Imaging. Neurosurgery. Aug; 2013 73(2):262–270. [PubMed: 23615081]
17. Akpek S, Brunner T, Benndorf G, Strother C. Three-dimensional imaging and cone beam volume CT in C-arm angiography with flat panel detector. Diagnostic and interventional radiology (Ankara, Turkey). Mar; 2005 11(1):10–13.
18. Doelken M, Struffert T, Richter G, et al. Flat-panel detector volumetric CT for visualization of subarachnoid hemorrhage and ventricles: preliminary results compared to conventional CT. Neuroradiology. Jun; 2008 50(6):517–523. [PubMed: 18330518]
19. Heller RS, Malek AM. Successful detection of embologenic ulceration in a symptomatic non-hemodynamic intracranial stenosis using C-arm cone beam CT. Journal of neurointerventional surgery. Mar.2013 5(2):e3. [PubMed: 22266793]
20. Rahal JP, Malek AM. Benefit of cone-beam computed tomography angiography in acute management of angiographically undetectable ruptured arteriovenous malformations. Journal of neurosurgery. May 17.2013
21. Wegner RE, Oysul K, Pollock BE, et al. A modified radiosurgery-based arteriovenous malformation grading scale and its correlation with outcomes. International journal of radiation oncology, biology, physics. Mar 15; 2011 79(4):1147–1150.
22. Fujimoto M, Uno J, Ikai Y, et al. Risk of rebleeding in arteriovenous malformations due to impaired venous drainage after radiosurgery. Neurologia medico-chirurgica. 2011; 51(8):585–587. [PubMed: 21869582]
23. Maruyama K, Kawahara N, Shin M, et al. The risk of hemorrhage after radiosurgery for cerebral arteriovenous malformations. The New England journal of medicine. Jan 13; 2005 352(2):146–153. [PubMed: 15647577]
24. Maruyama K, Shin M, Tago M, et al. Management and outcome of hemorrhage after Gamma Knife surgery for arteriovenous malformations of the brain. Journal of neurosurgery. Dec; 2006 105(Suppl):52–57. [PubMed: 18503330]
25. Flickinger JC, Pollock BE, Kondziolka D, Lunsford LD. A dose-response analysis of arteriovenous malformation obliteration after radiosurgery. International journal of radiation oncology, biology, physics. Nov 1; 1996 36(4):873–879.
26. Hamm KD, Klisch J, Surber G, Kleinert G, Eger C, Aschenbach R. Special aspects of diagnostic imaging for radiosurgery of arteriovenous malformations. Neurosurgery. May; 2008 62(5 Suppl):A44–52. discussion A52. [PubMed: 18580780]
27. Zhang XQ, Shirato H, Aoyama H, et al. Clinical significance of 3D reconstruction of arteriovenous malformation using digital subtraction angiography and its modification with CT information in stereotactic radiosurgery. International journal of radiation oncology, biology, physics. Dec 1; 2003 57(5):1392–1399.
28. Kondziolka D, Lunsford LD, Kanal E, Talagala L. Stereotactic magnetic resonance angiography for targeting in arteriovenous malformation radiosurgery. Neurosurgery. Oct; 1994 35(4):585–590. discussion 590-581. [PubMed: 7808600]
29. Stock KW, Radue EW, Jacob AL, Bao XS, Steinbrich W. Intracranial arteries: prospective blinded comparative study of MR angiography and DSA in 50 patients. Radiology. May; 1995 195(2): 451–456. [PubMed: 7724765]
30. Ehricke HH, Schad LR, Gademann G, Wowra B, Engenhart R, Lorenz WJ. Use of MR angiography for stereotactic planning. Journal of computer assisted tomography. Jan-Feb;1992 16(1):35–40. [PubMed: 1729304]
31. Duran M, Schoenberg SO, Yuh WT, Knopp MV, van Kaick G, Essig M. Cerebral arteriovenous malformations: morphologic evaluation by ultrashort 3D gadolinium-enhanced MR angiography. European radiology. Dec; 2002 12(12):2957–2964. [PubMed: 12439576]

32. Unlu E, Temizoz O, Albayram S, et al. Contrast-enhanced MR 3D angiography in the assessment of brain AVMs. European journal of radiology. Dec; 2006 60(3):367–378. [PubMed: 16965882]
33. Vermandel M, Betrouni N, Pasquier D, Gauvrit J, Vasseur C, Rousseau J. A 2D/3D matching based on a hybrid approach: improvement to the imaging flow for AVM radiosurgery. Conf Proc IEEE Eng Med Biol Soc. 2005; 3:3071–3073. [PubMed: 17282892]
34. Conti A, Pontoriero A, Farago G, et al. Integration of three-dimensional rotational angiography in radiosurgical treatment planning of cerebral arteriovenous malformations. International journal of radiation oncology, biology, physics. Nov 1; 81(3):e29–37.
35. Colombo F, Cavedon C, Francescon P, et al. Three-dimensional angiography for radiosurgical treatment planning for arteriovenous malformations. Journal of neurosurgery. Mar; 2003 98(3): 536–543. [PubMed: 12650425]
36. Kakizawa Y, Nagashima H, Oya F, et al. Compartments in arteriovenous malformation nidi demonstrated with rotational three-dimensional digital subtraction angiography by using selective microcatheterization. Report of three cases. Journal of neurosurgery. Apr; 2002 96(4):770–774. [PubMed: 11990820]
37. Bridcut RR, Winder RJ, Workman A, Flynn P. Assessment of distortion in a three-dimensional rotational angiography system. The British journal of radiology. Mar; 2002 75(891):266–270. [PubMed: 11932221]
38. Colombo F, Cavedon C, Casentini L, Francescon P, Causin F, Pinna V. Early results of CyberKnife radiosurgery for arteriovenous malformations. Journal of neurosurgery. Oct; 2009 111(4):807–819. [PubMed: 19344220]
39. Kamran M, Nagaraja S, Byrne JV. C-arm flat detector computed tomography: the technique and its applications in interventional neuro-radiology. Neuroradiology. Apr; 52(4):319–327. [PubMed: 19859702]
40. Engelhorn T, Struffert T, Richter G, et al. Flat panel detector angiographic CT in the management of aneurysmal rupture during coil embolization. AJNR. American journal of neuroradiology. Sep; 2008 29(8):1581–1584. [PubMed: 18499792]
41. Psychogios MN, Schramm P, Buhk JH, et al. Angiographic CT after intravenous contrast agent application: A noninvasive follow-up tool after intracranial angioplasty and stenting. AJNR. American journal of neuroradiology. Nov; 31(10):1886–1891. [PubMed: 20634309]
42. Irie K, Murayama Y, Saguchi T, et al. Dynact soft-tissue visualization using an angiographic C-arm system: initial clinical experience in the operating room. Neurosurgery. Mar; 2008 62(3 Suppl 1):266–272. discussion 272. [PubMed: 18424996]
43. Radvany MG, Ehtiati T, Huang J, Mahesh M, Gailloud P. Aortic arch injection with C-arm cone beam CT for radiosurgery treatment planning of cerebral arteriovenous malformations: technical note. Journal of neurointerventional surgery. Oct 22.
44. Ott S, Struffert T, Hertel V, et al. Visualization and monitoring of acute epistaxis during endovascular treatment using a flat detector CT. Minim Invasive Neurosurg. Aug; 54(4):187–190. [PubMed: 21922449]
45. Mordasini P, El-Koussy M, Brekenfeld C, et al. Applicability of Tableside Flat Panel Detector CT Parenchymal Cerebral Blood Volume Measurement in Neurovascular Interventions: Preliminary Clinical Experience. AJNR. American journal of neuroradiology. Oct 27.
46. Psychogios MN, Buhk JH, Schramm P, Xyda A, Mohr A, Knauth M. Feasibility of angiographic CT in peri-interventional diagnostic imaging: a comparative study with multidetector CT. AJNR. American journal of neuroradiology. Aug; 31(7):1226–1231. [PubMed: 20360343]
47. Douglas JG, Goodkin R. Treatment of arteriovenous malformations using Gamma Knife surgery: the experience at the University of Washington from 2000 to 2005. Journal of neurosurgery. Dec; 2008 109(Suppl):51–56. [PubMed: 19123888]
48. Fokas E, Henzel M, Wittig A, Grund S, Engenhart-Cabillic R. Stereotactic radiosurgery of cerebral arteriovenous malformations: long-term follow-up in 164 patients of a single institution. Journal of neurology. Aug; 2013 260(8):2156–2162. [PubMed: 23712798]
49. Parkhutik V, Lago A, Aparici F, et al. Late clinical and radiological complications of stereotactical radiosurgery of arteriovenous malformations of the brain. Neuroradiology. Mar; 2013 55(4):405–412. [PubMed: 23183855]

50. Flickinger JC, Kondziolka D, Lunsford LD, et al. Development of a model to predict permanent symptomatic postradiosurgery injury for arteriovenous malformation patients. Arteriovenous Malformation Radiosurgery Study Group. International journal of radiation oncology, biology, physics. Mar 15; 2000 46(5):1143–1148.
51. Yen CP, Khaled MA, Schwyzer L, Vorsic M, Dumont AS, Steiner L. Early draining vein occlusion after gamma knife surgery for arteriovenous malformations. Neurosurgery. Nov; 2010 67(5): 1293–1302. discussion 1302. [PubMed: 20871437]
52. Ding D, Yen CP, Xu Z, Starke RM, Sheehan JP. Radiosurgery for patients with unruptured intracranial arteriovenous malformations. Journal of neurosurgery. May; 2013 118(5):958–966. [PubMed: 23530863]
53. Parkhutik V, Lago A, Tembl JI, et al. Postradiosurgery hemorrhage rates of arteriovenous malformations of the brain: influencing factors and evolution with time. Stroke; a journal of cerebral circulation. May; 2012 43(5):1247–1252.
54. Yen CP, Sheehan JP, Schwyzer L, Schlesinger D. Hemorrhage risk of cerebral arteriovenous malformations before and during the latency period after GAMMA knife radiosurgery. Stroke; a journal of cerebral circulation. Jun; 2011 42(6):1691–1696.
55. Yamamoto M, Jimbo M, Ide M, et al. Gamma knife radiosurgery for cerebral arteriovenous malformations: an autopsy report focusing on irradiation-induced changes observed in nidus-unrelated arteries. Surgical neurology. Nov; 1995 44(5):421–427. [PubMed: 8629225]

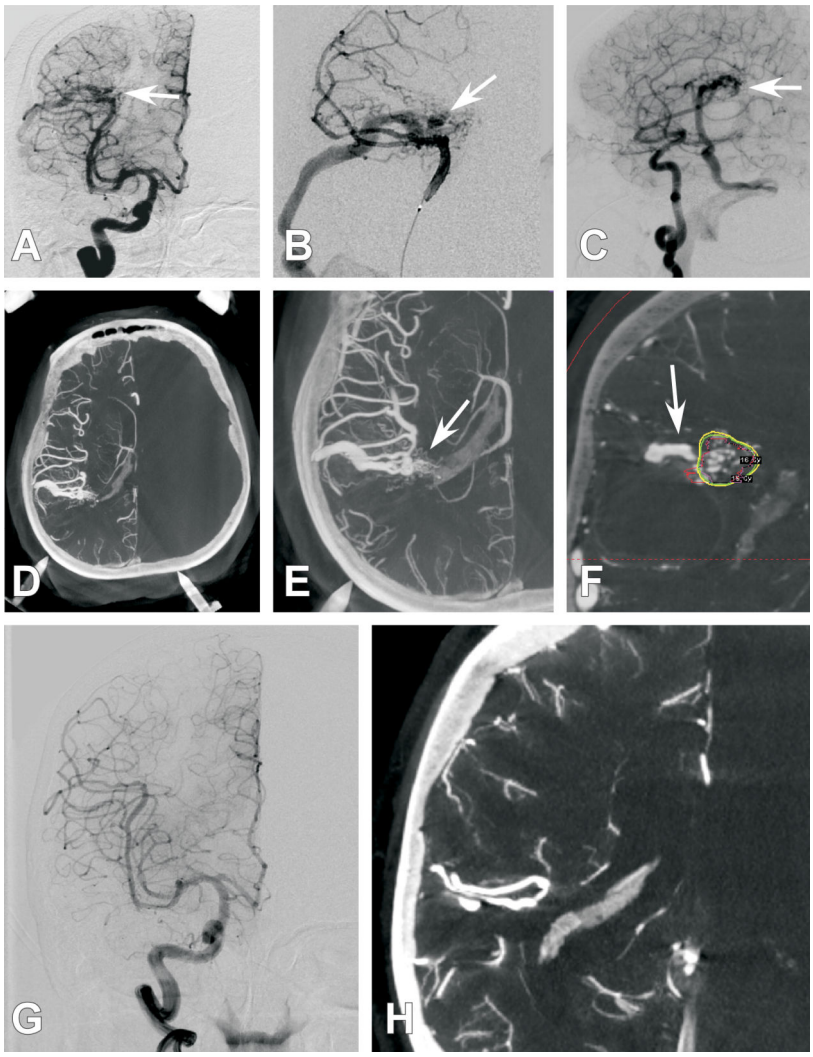

Figure 1. Case 4

A 61-year old female presented with a right parietal hemorrhage, generalized tonic clonic seizure, and left hemiparesis. She was found to harbor an AVM at the site of hemorrhage and was treated with GKR 1 month after presentation. Several diagnostic cerebral angiogram images are presented. **A.)** Anterio-posterior (AP) projection of an internal carotid artery (ICA) injection. Poor detailed arterial, nidal, and venous resolution of the AVM are noted (White arrow). **B.)** Anterio-posterior (AP) projection of a selective middle cerebral artery (MCA) injection. Poor detailed arterial, nidal, and venous resolution of the AVM are noted (White arrow). **C.)** 3DRA right ICA injection with a right parietal AVM (white arrow) but with continued limited arterial, nidal, and venous anatomy. **D.)** Axial CBCT-A reconstruction with patient in the Leksell head frame. The anterior posts and posterior pins of the frame are seen. A right parietal AVM is visualized. **E.)** Magnified axial CBCT-A reconstruction. Excellent resolution of the complex arterial and venous structure of the AVM are noted (White arrow). **F.)** Screen shot image of a coronal CBCT-A reconstruction uploaded for planning on the Leksell stereotactic planning computer. The radiated field is demonstrated by the encircled areas at different radiation isodoses. Note that the draining

vein is easily resolved and left out of the radiation field (White arrow). **G.)** 2-year follow-up AP projection of an ICA injection demonstrating complete obliteration of the previously seen AVM. **H.)** 2-year follow-up magnified axial CBCT-A reconstruction demonstrating complete obliteration of the previously seen AVM.

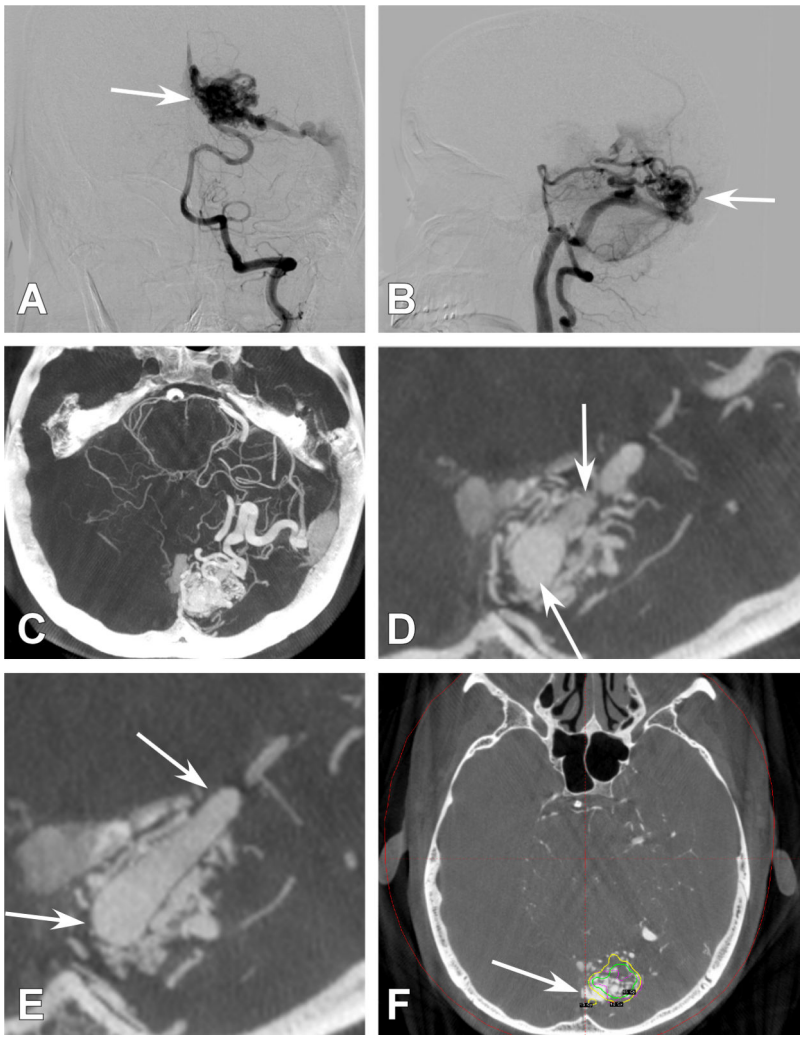

Figure 2. Case 6

A 41-year old male presented with a generalized tonic clonic seizure. A left occipital AVM was appreciated. **A.)** Anterio-posterior (AP) projection of a left vertebral artery (VA) injection. White arrow demonstrates an AVM with poor detailed arterial, nidal, and venous resolution. **B.)** 3DRA left VA injection demonstrates the AVM (white arrow) but with continued limited arterial, nidal, and venous anatomy. **C.)** Axial CBCT-A reconstruction with patient in the Leksell headframe. A detailed view of the left occipital AVM is demonstrated. **D.)** Magnified axial CBCT-A reconstruction. Exquisite detail of the vasculature can be seen with the arterial feeders emptying into the draining vein (White arrow). **E.)** Magnified axial CBCT-A reconstruction once again demonstrating high resolution and visualization of the feeding artery anatomy and its abnormal connections with the draining vein (white arrow). **F.)** Screen shot image of an axial CBCT-A reconstruction uploaded for planning on the Leksell stereotactic planning computer. The radiated field is demonstrated by the encircled areas at different radiation isodoses. Note that the draining vein is easily resolved and minimal radiation is given to this structure (White arrow).

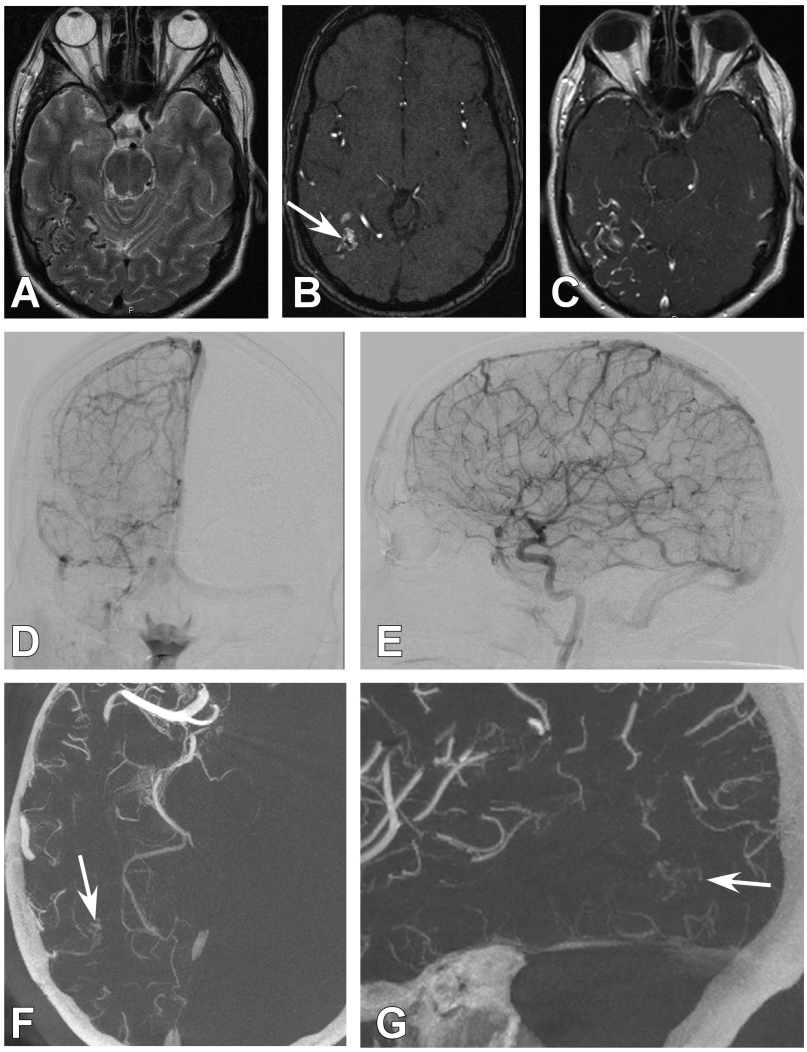

Figure 3. Case 21

A 52-year old male presented with a generalized tonic clonic seizure. A right parietal AVM was discovered. **A.)** Axial T2-weighted magnetic resonance imaging (MRI) demonstrating flow voids consistent with an AVM in the right parietal area. **B.)** Axial magnetic resonance angiography time of flight (MRA-TOF) images demonstrated an AVM nidus (White arrow). **C.)** Axial T1-weighted post contrast MRI demonstrates poor resolution of feeding artery and nidal anatomy. **D.)** Anterio-posterior (AP) projection of a right internal carotid artery (ICA). The AVM was unable to be resolved. **E.)** 3DRA right ICA injection. The AVM is not visualized. **F.)** Axial CBCT-A reconstruction with patient in the Leksell head frame. A detailed view of the small right parietal AVM is demonstrated (White arrow). **G.)** Sagittal CBCT-A reconstruction with a detailed view of the small right parietal AVM. (White arrow).

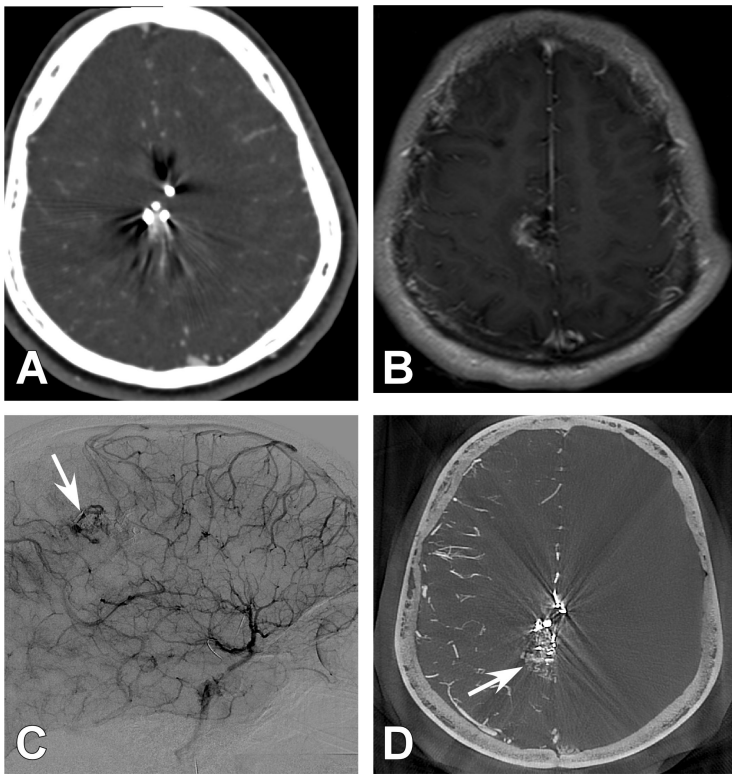

Figure 4. Case 2

A 20-year old male presented for AVM treatment after 3 prior outside hospital embolizations. All imaging was obtained on the same day **A.)** Axial computed tomography angiography (CTA) demonstrating previously embolized AVM. No residual nidus is visualized. There is significant starburst artifact **B.)** Axial magnetic resonance angiography (MRA) demonstrating embolization material. Faint residual nidus is visualized but resolution is poor. **C.)** Lateral right internal carotid artery (ICA) injection demonstrating embolic material (white arrow). It is unclear whether residual nidus exists. **D.)** Axial CBCT-A demonstrating embolized AVM. Clear residual nidus is seen (white arrow). Embolized AVM is much more hyperdense and easily delineated from residual AVM.

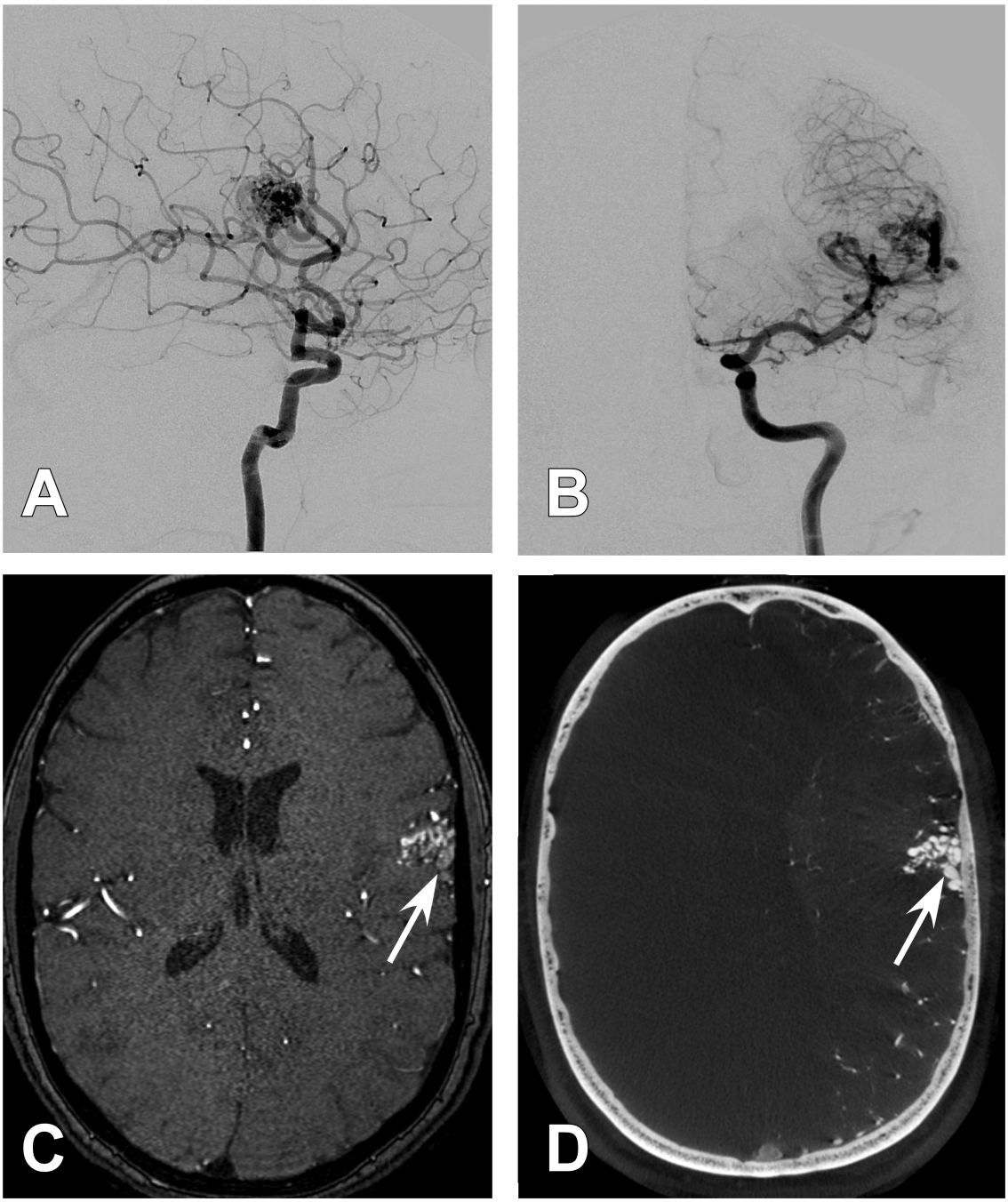

Figure 5. Case 10

A 33-year old female presented with seizure. A left frontal AVM was demonstrated. Magnetic resonance angiography (MRA) and CBCT-A were obtained on the same day. **A.)** Lateral left internal carotid artery (ICA) injection demonstrating an AVM. No clear nidal anatomy can be distinguished. **B.)** Anterioposterior (AP) left ICA injection demonstrating AVM. Once again no clear nidal anatomy is appreciated. **C.)** Axial MRA demonstrating AVM nidus. Little detail is appreciated concerning the nidal anatomy. White arrow points to any area of slower flow possibly representing venous drainage. **D.)** Axial CBCT-A

demonstrating detailed nidal anatomy. White arrow clearly reveals this structure is a draining vein.

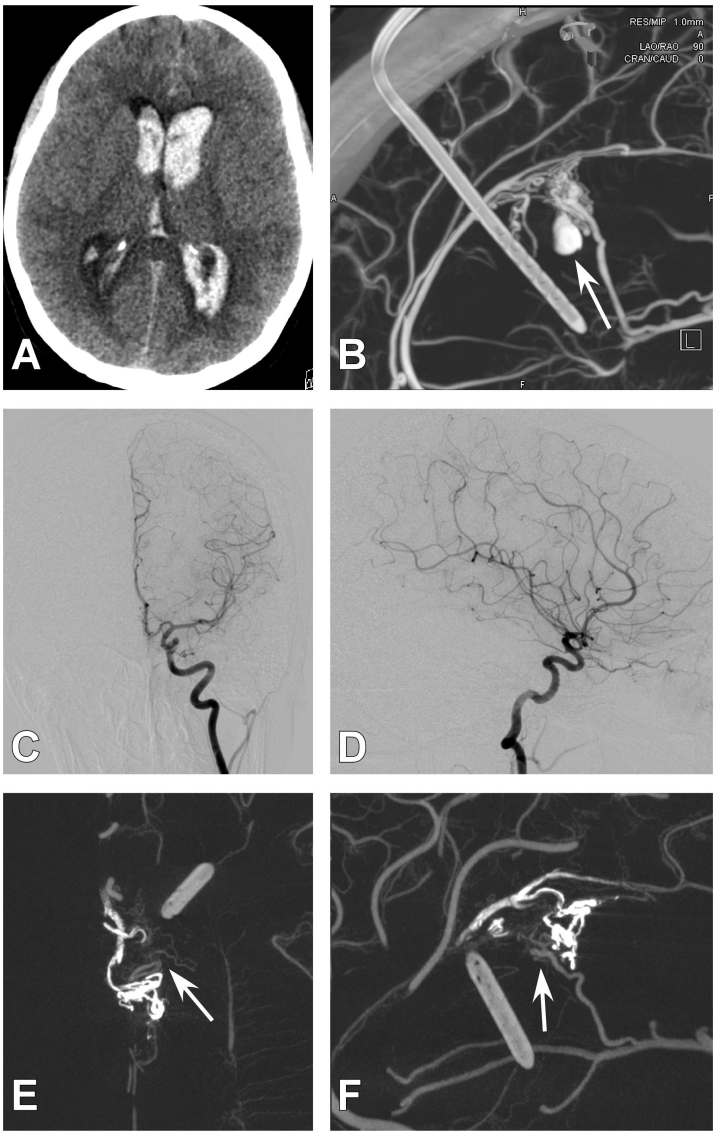

Figure 6. Case 22

A 26-year old female presented with a hemorrhage. **A.)** Axial computed tomography (CT) demonstrating intraventricular hemorrhage. **B.)** Initial CBCT-A demonstrating a left pericallosal AVM with an 8-mm intranidal aneurysm. Exquisite detail is appreciated about the nidal anatomy. This AVM was subsequently embolized **C.)** 4-month follow-up anterioposterior (AP) injection of the right internal carotid artery (ICA) demonstrating no apparent residual AVM. **D.)** 4-month lateral ICA injection of the right ICA demonstrating no apparent residual AVM. **E.)** Axial CBCT-A image demonstrating embolic material that is hyperdense as well as residual AVM filling (white arrow). **F.)** Sagittal CBCT-A image demonstrating embolic material as well as residual nidus filling (white arrow).

Table 1

Comparison of Modalities used for Stereotactic Radiosurgery planning for treatment of AVMs

Modality	Advantages	Limitations
CTA	1.) Non-invasive 2.) 3D-visualization and reconstruction 3.) Improved spatial resolution in comparison to MRA	1.) Large contrast bolus 2.) Temporal resolution not possible 3.) Heavily affected by metal or embolic material artifact causing a star-burst appearance
MRA	1.) Non-invasive 2.) 3D-visualization and reconstruction 3.) No associated radiation 4.) Contrast is not necessary in Time of Flight MRA	1.)Prone to clip artifact 2.) Poor spatial resolution 3.) Lesion visualization dependent on flow rate 4.) Temporal resolution not possible 5.) Long acquisition time
DSA	1.) Improved spatial resolution compared to CTA or MRA 2.) Presence of temporal resolution 3.) Can subselect compartments of AVM	1.) 2-D visualization (projections) of a 3-D lesion 2.) Prone to error in nidus size and shape delineation 3.) 2-D nature leads to over inclusion of healthy adjacent tissue in treatment
3DRA	1.) 3D-Visualization and reconstruction 2.) Improved spatial resolution of lesion anatomy and filling patterns compared to DSA 3) Venous phase potentially not well visualized	1.)Inability to incorporate fiducial frame into data set in some systems 2.) Must be fused with another data set for treatment
CBCT-A	1.) Higher spatial resolution of intracranial vasculature 2.) Higher sensitivity for lesions than DSA or 3DRA 3.) 3D-visualization and reconstruction 4.) Ability to incorporate frame into data set 5.)Can be applied to 3D data sets and multi-planar reconstruction	1.) Heavily affected by metal or embolic material artifact causing a star-burst appearance 2.) Longer acquisition time than 3DRA or DSA 3.) Degraded by Patient movement

* 3DRA- 3D-Rotational Angiography; CBCT-A- Cone Beam Computed Tomography Angiography; CTA- Computed Tomogrophy Angiography; DSA- Digital Subtraction Angiography; MRA - Magnetic Resonance Angiography

Table 2

Demographics and AVM Characteristics of Patients

Case #	Age (Years)	Sex	Presentation	Prior Treatment?	Nidus Size (cm)	Anatomical Location	SM Grade/RBAS	GKR Dose(Gy)*
1	56	M	Hemorrhage	N	1.0	Left Postcentral Gyrus	2/1.22	13
2	20	M	Hemorrhage	Embolization	2.0	Right Precentral Gyrus	2/0.58	12
3	36	M	Headaches	N	3.0	Right Precentral Gyrus	3/1.03	15
4	61	F	Hemorrhage	Proton Beam	1.5	Right Temporparietal	2/1.37	15
5	19	M	Incidental; Epistaxis	N	1.8	Left Postcentral Gyrus	2/0.44	15
6	41	M	Seizure	N	2.0	Left Occipital	3/1.08	13
7	30	M	Hemorrhage	N	3.0	Right Precentral Gyrus	3/0.91	15
8	57	F	Seizure	N	1.0	Left Temporal	2/1.17	14
9	44	F	Headache	N	2.9	Right Parietal	2/1.83	16
10	33	F	Seizure	N	1.5	Left Frontal	2/0.72	14
11	57	M	Hemorrhage	N	1.0	Left Temporal	3/1.32	16
12	54	F	Seizure	N	4.5	Left Precentral Gyrus	3/1.4	13
13	45	M	Hemorrhage	N	2.5	Left Precentral Gyrus	3/1.14	16
14	61	M	Incidental; dysarthria	N	1.5	Right Temporal	1/1.27	16
15	44	M	Seizure		2	Right Temporal	2/1.44	17
16	46	F	Hemorrhage	Embolization	3.1	Right Cerebellar	2/1.03	16
17	47	F	Hemorrhage	N	1.0	Right Occipital	3/0.99	20
18	57	F	Headache	Proton Beam	1.8	Left Precentral Gyrus	2/1.27	16
19	28	M	Seizure	N	4	Right Precentral Gyrus	2/1.71	15
20	47	M	Seizure	N	4	Right Temporal	4/2.14	15
21	52	M	Seizure	N	1.5	Right Parietal	2/1.06	18
22	26	F	Hemorrhage	Embolization	1.5	Left Pericallosal	3/0.59	20

*Treatment dose given at the 50% isodose line. RBAS: Modified Radiosurgery Based AVM Grading Scale; SM: Spetzler-Martin; GKR: Gamma Knife Radiosurgery Gy: Gray

Table 3

Clinical and Radiographic outcome of Patients

Case #	Follow-Up (Month)	Clinical Outcome	Hemorrhage/Seizure post-treatment	Change in size of AVM	MRI T2 change
1	6	Improved Headache and Balance	N/N	Obliterated on MRA awaiting DCA	None
2	None	N/A	N/A	N/A	N/A
3	28	Decreased Headache	N/N	Decreased on MRI	Improved
4	37	Decreased Headache	N/N	Obliterated on DCA	None
5	24	No change (Incidental)	N/N	Obliterated on MRA	No change
6	39	Significantly improved Seizure control	N/N	Decreased on DCA	No Change
7	30	Improved Seizure Control	N/N	Decreased on DCA	None
8	21	Increased Seizure	N/Y	Decreased on CTA and MRA	None
9	27	Increased Seizure	N/Y	Decreased on MRA	Yes, improving
10	7	Decreased Headache	N/Y	Stable AVM size	None
11	25	Decreased Headache	N/N	Obliterated on DCA	Improved
12	2	Improved Headache	N/N	Stable AVM size	None
13	16	Improved Right Sided strength and Headaches	N/Y	Obliterated on DCA	None
14	None	N/A	N/A	N/A	N/A
15	19	Resolution of Seizures	N/N	Decreased on MRA	None
16	13	Improved Headaches	N/N	Stable on MRA	None
17	9	Improved cognition and Headaches	N/N	Decreased on CTA	N/A
18	6	Improved Headache	N/N	Decreased on MRA	No
19	6	Improved Seizure control	N/N	Decreased on CTA and MRA	No
20	5	Improved Seizure control	N/N	Decreased on DCA	No
21	Pending	N/A	N/A	N/A	N/A
22	Pending	N/A	N/A	N/A	N/A

CTA-Computed tomography angiography; DCA-Diagnostic Cerebral Angiogram; MRI-Magnetic resonance angiography